# Spectroscopic Tools Applied to Flerovium Decay Chains

**D.M. Cox[†], A. Såmark-Roth[†], D. Rudolph[†], L.G. Sarmiento[†], C. Fahlander[†], U. Forsberg[†], P. Golubev[†], J.A.M. Heery[$], A. Yakushev[‡], H. M. Albers[‡], M. Block[‡§¶], H. Brand[‡], R.M. Clark[°], Ch.E. Düllmann[‡§¶], J. Eberth[◇], J.M. Gates[°], F. Giacoppo[‡§], M. Götz[‡§¶], S. Götz[‡§¶], R.-D. Herzberg[$], E. Jäger[‡§], B. Kindler[‡] J. Khuyagbaatar[‡], I. Kojouharov[‡], J.V. Kratz[¶], J. Krier[‡], N. Kurz[‡], L. Lens[‡§¶], B. Lommel[‡] A. Mistry[‡], C.-C. Meyer[‡], C. Mokry[¶], P. Papadakis[$], J.L. Pore[°], J. Runke[‡§], P. Thörle-Pospiech[§¶], N. Trautmann[¶], H, Schaffner[‡], B. Schausten[‡], J. Uusitalo[*]**

[†]Department of Physics, Lund University, SE-22100 Lund, Sweden
[$]Department of Physics, University of Liverpool, Liverpool L69 7ZE, United Kingdom
[‡]GSI Helmholtzzentrum für Schwerionenforschung GmbH, D-64291, Darmstadt, Germany
[§]Helmholtz Institute Mainz, D-55099 Mainz, Germany
[¶]Institut für Kernchemie, Johannes Gutenberg-Universität Mainz, D-55099 Mainz, Germany
[°]Lawrence Berkeley National Laboratory, Berkeley, California 94720-8169, USA
[◇]Institut für Kernphysik, Universität zu Köln, D-50937 Cologne, Germany
[*]Department of Physics, University of Jyväskylä, FI-40014 Jyväskylä, Finland

E-mail: daniel.cox@nuclear.lu.se

September 2019

**Abstract.** An upgraded TASISpec setup, with the addition of a veto DSSD and the new Compex detector-germanium array, has been employed with the gas-filled recoil separator TASCA at the GSI Helmholtzzentrum für Schwerionenforschung Darmstadt, to study flerovium (element 114) decay chains. The detector upgrades along with development of new analytical techniques have improved the sensitivity of the TASISpec setup for measuring $\alpha$-photon coincidences. These improvements have been assessed with test reactions. The reaction $^{48}$Ca+$^{206,207}$Pb was used for verification of experimental parameters such as transmission to implantation DSSD and target-segment to $\alpha$-decay correlations. The reaction $^{48}$Ca+$^{nat}$Hf was used to produce several short-lived nuclei with multiple-$\alpha$ decay chains to investigate pile-up event deconvolution.

Content from this work may be used under the terms of the Creative Commons Attribution 3.0 licence. Any further distribution of this work must maintain attribution to the author(s) and the title of the work, journal citation and DOI.
Published under licence by IOP Publishing Ltd

## 1. Introduction

For a number of decades, great effort has been put into expanding the nuclear landscape to heavier masses [1]. This has largely revolved around the use of fusion-evaporation reactions using $^{48}$Ca beams on actinide targets [2, 3]. As the nuclei being sought have become heavier, their production cross-sections have decreased. This has posed a problem for studying these nuclei as standard spectroscopic approaches struggle when the production rate falls below one atom a day, a week or even longer. Significant developments of new detector setups and analysis techniques are required to overcome this challenge. The results presented here are based on the experiment U310, with the aim to study flerovium decay chains using the reaction $^{48}$Ca+$^{242,244}$Pu. The measurements were performed in 2019 at the TASCA beam line at the GSI Helmholtzzentrum für Schwerionenforschung, Darmstadt, Germany, in the frame of FAIR Phase-0.

The previous experiment employing the multicoincidence particle-photon decay station TASISpec [4] at the gas filled recoil separator TASCA [5] was performed in 2012 [6, 7, 8]. Since then, a number of infrastructure changes have occured. Power supplies for the quadrupole magnets were replaced and a new shield wall between the separator and focal plane was constructed requiring TASISpec be moved downstream with respect to the focal plane of TASCA. As the main experiment employed a target wheel containing $^{242}$Pu and $^{244}$Pu segments it was important to correlate each implantation event with a specific segment. The reaction $^{48}$Ca+$^{206,207}$Pb was used to reassure the transmission of fusion-evaporation recoils from the target to the focal plane of TASCA and to validate target segment assignment. This is detailed in Sec. 2.

TASISpec has been equipped with a veto detector behind the implantation double-sided silicon strip detector (DSSD), described in Sec. 3.1. A target of $^{nat}$Hf was used to produce nuclei in the region of $^{221}$Th where there are several long $\alpha$-decay chains with half-lives down to sub-microsecond. The analysis of these multiple-event traces is detailed in Sec. 3.2. Further results of studying $\alpha$-photon coincidences in this region will be reported elsewhere.

The germanium-detector array of TASISpec has been upgraded with new Compex germanium detectors which are briefly described in the current work and will be reported in detail elsewhere. To minimise background radiation, passive shields have been installed in the TASCA cave. Within the new environment, expected random photon rates during different beam conditions have been analysed and are described in Sec. 4.2.

## 2. Validation of Experimental Parameters

The $^{48}$Ca+$^{206,207}$Pb fusion-evaporation reaction was utilised at an energy of 4.72 MeV/A with $\sim$2.2 µm thin Al degraders for means of validation of experimental parameters. Correlations based on the criteria in Table 1 were used to extract the $^{252,253}$No yields for a number of quadrupole magnet settings and for the different target segments.

Table 1: Search criteria for correlations between implanted $^{252,253}$No nuclei and their subsequent $\alpha$ or spontaneous fission decays. The criteria include $\alpha$-particle and fission energies and correlation times between implant and decay. Restrictions concerning beam status are indicated.

| | $^{252}$No | $^{253}$No | Beam |
|---|---|---|---|
| $E_{\text{imp}}$ | $[10, 20]$ MeV | $[10, 20]$ MeV | ON |
| $E_{\alpha}$ | $[8.3, 8.6]$ MeV | $[8.0, 8.3]$ MeV | OFF |
| $E_{\text{fission}}$ | $[100, 250]$ MeV | - | OFF |
| $\Delta t_{\text{imp}-\alpha_1/\text{fission}}$ | $[0,\ 14]$ s | $[0,\ 300]$ s | - |

Besides a well established B$\rho = 2.10$ Tm, a number of different quadrupole settings centred around the previously optimal setting of (525 A, 510 A) [7] were evaluated. Integrated beam doses were used for normalisation and the resulting yields for the quadrupole magnet settings are presented in Table 2(a). The yield from the previously established optimal settings and (520 A, 515 A) were comparable. The former magnet settings were chosen and used for the remainder of the experiment.

With each beam pulse a so-called *target bit* signal is included in the data stream to allow correlation between target segment and implant and thus subsequent $\alpha$ decays. A target wheel comprising four segments, with two each of $^{207}$Pb and $^{206}$Pb was used. The yield of $^{252}$No, compared to the total $^{252,253}$No yields, for each target bit is presented in Table 2(b). The result shows that target bits 1 and 2 yield the highest fraction of $^{252}$No, consistent with the composition of the four Pb target segments.

Table 2: $^{252,253}$No-production yield for different TASCA quadrupole magnet settings (a) and target segments (b).

(a)

| Quadrupoles (A, A) | 525, 505 | 520, 515 | 525, 510 | 530, 515 | 540, 515 |
|---|---|---|---|---|---|
| $^{252,253}$No yield | 131(3) | 138(4) | 133(2) | 128(3) | 112(3) |

(b)

| Target bit | Material | Degrader | $^{252}$No/$^{252,253}$No yield |
|---|---|---|---|
| 0 | $^{207}$Pb (0.942 mg/cm$^2$) | Al (2.29 µm) | 0.14 |
| 1 | $^{206}$Pb (0.958 mg/cm$^2$) | Al (2.19 µm) | 0.43 |
| 2 | $^{206}$Pb (1.012 mg/cm$^2$) | Al (2.05 µm) | 0.74 |
| 3 | $^{207}$Pb (0.961 mg/cm$^2$) | Al (2.23 µm) | 0.01 |

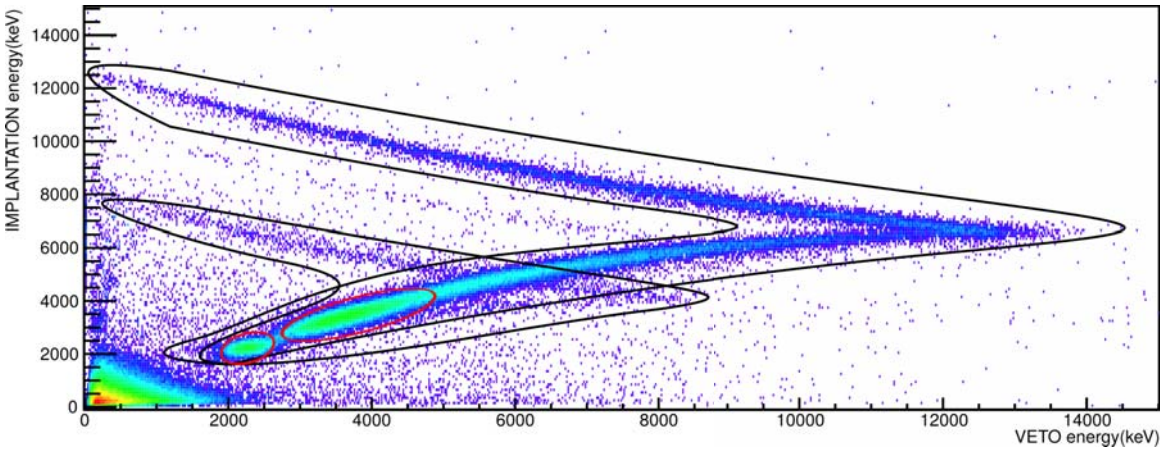


Figure 1: Veto-implantation identification plot with light-ion punch-through events (black) and directly scattered separator gas events (red) highlighted.

## 3. Silicon Detectors

TASISpec comprises an implantation DSSD surrounded by four further DSSDs in a box arrangement [4]. In the current experiment the implantation DSSD had a reduced thickness (310 µm instead of 520 µm [6]) and a second 310 µm DSSD positioned behind the implantation DSSD served as a veto detector.

### *3.1. Veto Detector*

The addition of a veto detector to TASISpec allows for a greater selectivity of events. Light-ion punch-through events and heavy-ion implantation events or $\alpha$-decay events can be distinguished. Another advantage is the ability to differentiate between escaping $\alpha$ particles and electron punch-through events. Figure 1 shows a veto-implantation identification plot. A number of features can be seen on this plot. Firstly there are *boomerang*-like shapes. These can be explained by light ions punching through first one detector and then the second detector as their energy is increased. Here the two detectors are functioning as a $\Delta E$-$E$ detector. Secondly at the lower energies there are two intense regions corresponding to separator gas scattered from target-like or beam-like particles.

### *3.2. Digital Signal Processing*

The preamplified signals of all channels in the Si-detectors were recorded in 80 µs traces using 14 bit, 50 MHz sampling ADCs, see e.g. Ref [9] for more details on data acquisition. To distinguish pile-up events created by, for example, two subsequent fast $\alpha$-decays, a digital sampling system is essential. Moving window deconvolution routines developed to handle single-pulse traces [7] and pile-up traces in previous work [10, 11] have been extended to further optimise the pulse identification in pile-up signals. With the new

routine it was possible to lower the energy limit for resolving pile-up signals from 900 keV down to 300 keV. The working principle of the new routine is illustrated in Fig. 2. The two-step method comprises the application of a second-order low-pass Butterworth digital filter and an algorithm to identify bipolar pulses in the second-derivative of the filtered signal. In this way, the routine is less sensitive to noise and still able to identify pile-up pulses. While the new routine is robust in the sense that only a few parameters are needed, it is not as effective as the previous pile-up routine in identifying pulses with a time difference of 10-50 trace samples (i.e. 0.2 µs-1.0 µs). The final combined routine utilises the routine best suited to the signal in question. For a detailed description of the routine, the reader is referred to the supplemental material Jupyter-notebook [12].

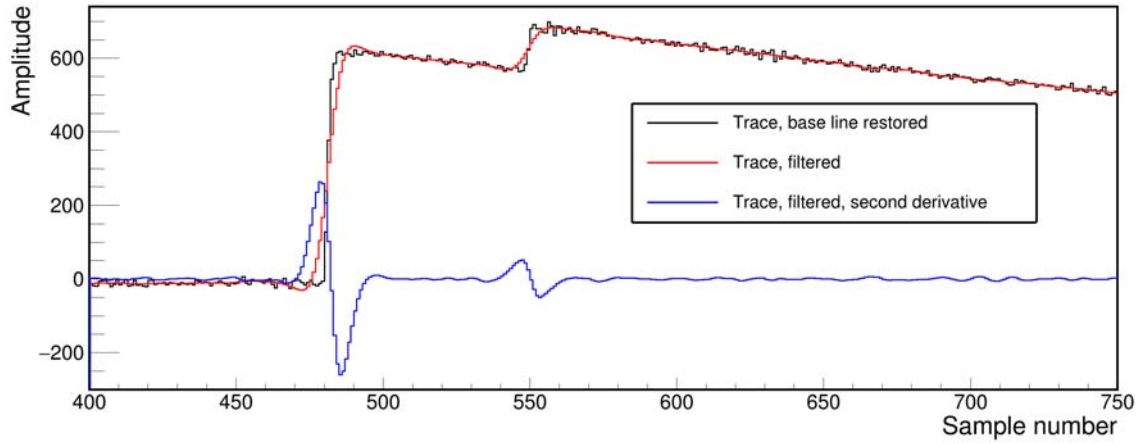


Figure 2: The original (black) and processed trace for filtering (red) and pile-up identification (blue). The trace, once calibrated, comprises a 2.5 MeV signal followed 1.4 µs later by a 0.5 MeV signal.

### *3.3. Particle Spectroscopy*

$^{133}$Ba and $^{207}$Bi calibration sources were used for initial calibration and threshold adjustment of the DSSDs. For the implantation DSSD, additionally, $\alpha$ decay of $^{252}$No nuclei was used for an in-beam calibration at relevant $\alpha$ energies. In the case of the higher energy point, $^{252}$No, a recoil fraction of 50% was used as a starting point (see below).

The energy of escaping $\alpha$-particles, interacting in both implantation and a box DSSD, is reconstructed using SRIM [13], calculated deadlayers, and geometrical factors [7]. The pixel-by-pixel deadlayer thicknesses for the new implantation DSSD were estimated and the reconstruction routine was optimised for the current data set. The result is presented in Fig. 3(a).

All channels in the implantation DSSD were recalibrated across the duration of the experiment. Two high-intensity, well separated peaks covering the energy range of interest, $^{213}$Po at 8.5 MeV and $^{212}$Po at 11.7 MeV, were used for the recalibration.

The calibrated total spectrum for the implantation DSSD during beam-OFF periods is presented in Fig. 3(b) and the achieved FWHM energy resolutions were 50 keV and 55 keV for the $^{213,212}$Po peaks, respectively.

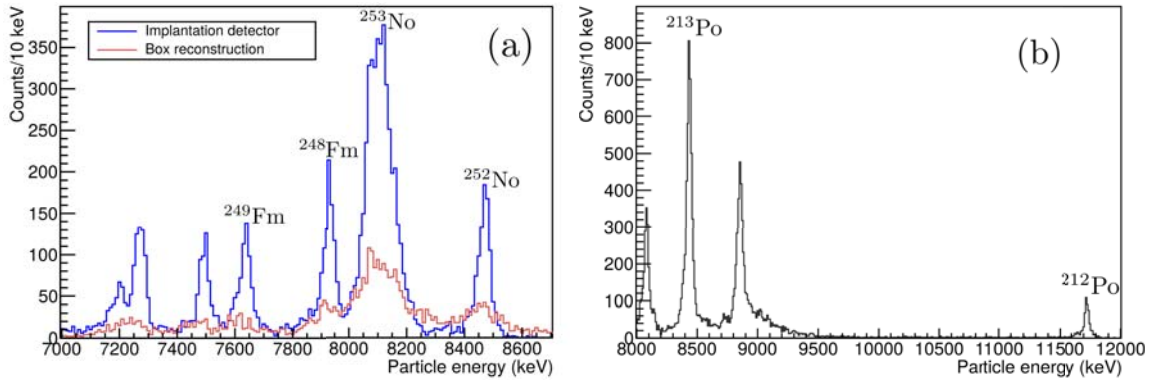


Figure 3: (a) Beam-OFF implantation DSSD (blue) and reconstructed box plus implantation (red) spectra in Pb-target measurements. (b) Beam-OFF implantation DSSD spectrum in $^{242,244}$Pu-target measurements. Recalibration peaks are labeled.

For implanted nuclei, the measured energy includes both the energy deposited by the $\alpha$ particle ($E_\alpha$) and the recoiling nucleus. Due to the large ionising potential of the recoiling nucleus, part of its energy is not recorded [14]. We assume that only a fraction, $r$, of the recoil energy of the decay product with mass number $A-4$ is detected ($E_{det}$).

$$E_{det} = E_\alpha \cdot \left(1 + \frac{4}{(A-4)} \cdot r\right) \tag{1}$$

The recoil fraction was determined by the investigation of multiple $\alpha$-decaying nuclei identified in the experiment. By comparing calculated recoil fractions with Eq. 1 and known $E_\alpha$-decay energies [15] a dependence on $Z^2$ of the decay product was concluded. Using a logarithmic fit to the data a general description of the recoil fraction was determined and the resulting $E_\alpha$ values lie within 10 keV of the tabulated data.

## 4. Germanium Detectors

The current version of TASISpec employed a Euroball-type cluster detector [16] along with four Compex detectors. Figure 4(a) shows the arrangement of the four Compex detectors around the TASISpec vacuum chamber. Each Compex detector consists of four individually encapsulated 5 cm x 5 cm x 5 cm cubic crystals in a common cryostat (Fig. 4(b)), and employing electrical cooling. A major advantage for this geometry is the proximity to the DSSDs possible and thus the angular coverage achievable.

### *4.1. Photon Spectroscopy*

Similar to the Si-detectors, all Ge-detector channels were processed with digital electronics. However, the preamplified signals were not recorded as traces during the

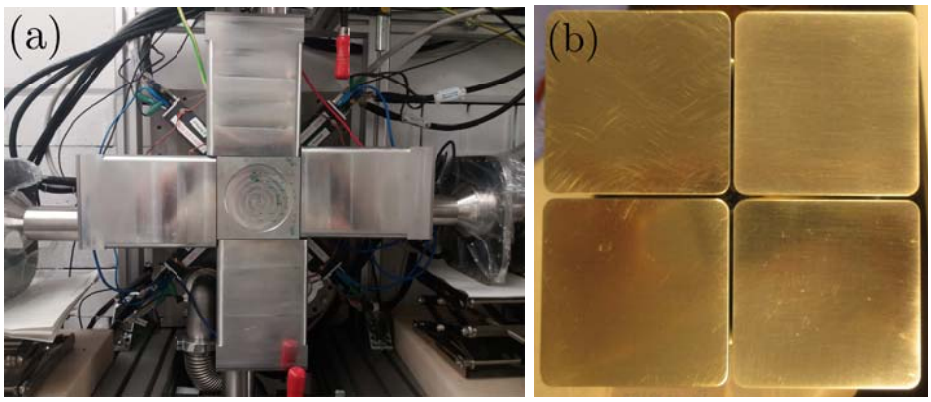


Figure 4: (a) Arrangement of four Compex detectors around the TASISpec vacuum chamber and (b) Compex detector with end-cap removed.

experiment. Instead FPGA software was applied to the signals to extract energy, baseline, and time. For best spectroscopic performance, the preamplifier decay constant for each detector was determined prior to the experiment. The Ge-detector data was further processed in line with what has been described in Refs. [17, 18].

### *4.2. Germanium Trigger Rates, Beam-ON/OFF*

Alongside the shielding wall constructed between the separator and focal plane, an additional *pre-chamber* has been added containing combined lead and paraffin shielding to further reduce background radiation.

To understand the expected background and random correlations of photons, dedicated measurements were taken with Ge-detectors triggering readout. The beam was pulsed at a rate of 5 Hz and at an intensity of 2.2 pμA on the Hf target. Figure 5 shows the rate of Ge-detector triggers as a function of time after the start of the beam pulse. It can be seen that the rate increases during the beam-ON pulse (5 ms) and then decreases exponentially. Comparing the trigger rates for different detectors, it is clear that the cluster, as expected due to greater angular coverage, receives the most radiation. The Compex detectors, regardless of position of the individual crystals within a detector, show a lower overall rate. Table 3 shows the average number of random photons within a 1 μs interval around particle trigger events as a function of time since the start of the beam pulse. The most important point is that, long after a beam-ON signal, such as when the beam has been shut off to watch for a decay chain, the random rate becomes increasingly small.

## 5. Summary

A number of upgrades both in the mechanical structure and analytical techniques have been detailed, including additional and upgraded detector systems along with techniques for digital trace processing and $\alpha$-particle energy correction. These upgrades will allow

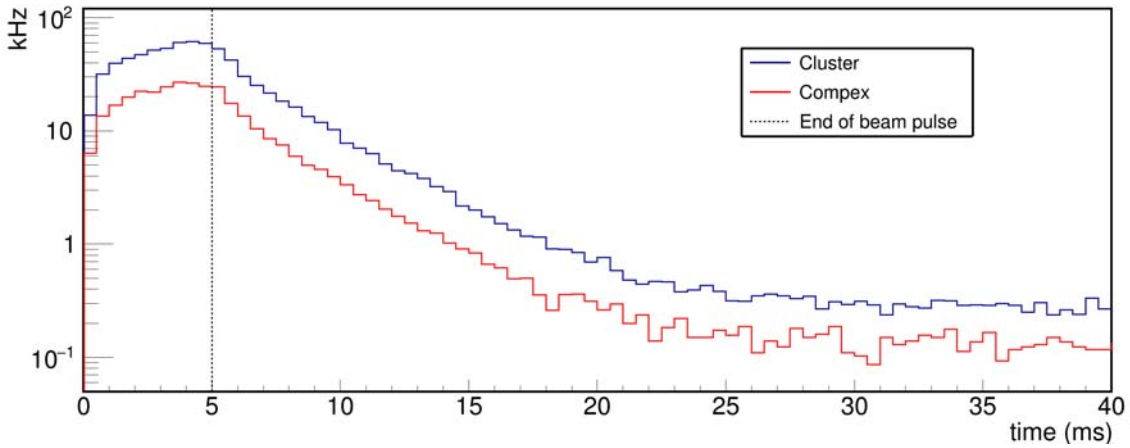


Figure 5: Ge-trigger rates as a function of the start of each beam pulse for different detectors. Beam-OFF is denoted by the dashed line at 5 ms.

Table 3: Expected number of random photons in the cluster and the four Compex Ge-detectors within a 1 µs time window for different intervals.

| | Beam ON | Beam OFF | |
|---|---|---|---|
| Detectors | $[0, 5]$ ms | $[15, 20]$ ms | $[100, 200]$ ms |
| Cluster (7 crystals) | $2.7 \cdot 10^{-1}$ | $7.0 \cdot 10^{-3}$ | $1.5 \cdot 10^{-4}$ |
| Compex (4x4 crystals) | $3.1 \cdot 10^{-1}$ | $7.8 \cdot 10^{-3}$ | $2.1 \cdot 10^{-4}$ |

for even greater $\alpha$-photon coincidence sensitivity with the TASISpec setup and form part of the ongoing development of the Lundium decay station.

## 6. Acknowledgements

The authors would like to thank the ion-source and the accelerator staff at GSI. This work has received funding from the European Union's Horizon 2020 research and innovation programme under grant agreement No. 654002 (ENSAR2) and is supported by the Royal Physiographic Society in Lund, the Swedish Research Council (VR 2016-3969), and the Knut and Alice Wallenberg foundation (KAW 2015.0021). The measurements were performed at the GSI Helmholtzzentrum für Schwerionenforschung, Darmstadt, Germany, in the frame of FAIR Phase-0.

## 7. References

[1] Düllmann, Ch.-E, Herzberg, R.-D, Nazarewicz, W, and Oganessian, Y, eds. *Special Issue on Superheavy Elements*, vol. 944. Nucl. Phys. A (2015)
[2] Oganessian, Yu Ts and Utyonkov, V. K. *Nucl. Phys. A*, 944:62–98 (2015)
[3] Rudolph, D, ed. *Chemistry and Physics of Heavy and Superheavy Elements*, vol. 131. EPJ Web of Conferences Proceedings (2016)
[4] Andersson, L-L, *et al. Nucl. Instrum. and Methods Phys. Res. A*, 622:164–170 (2010)

[5] Schädel, M. *Eur. Phys. J. D*, 45:67–74 (2007)
[6] Rudolph, D, *et al. Phys. Rev. Lett.*, 112502:1–5 (2013)
[7] Forsberg, U. *Ph.D. Thesis*. Lund University (2016). ISBN 9789176238127
[8] Forsberg, U, *et al. Nucl. Phys. A*, 953(953):117–138 (2016)
[9] Lorenz, Ch, *et al. Phys. Rev. C*, 99 (2019)
[10] Roth, A. *Masters Thesis*. Lund University (2016)
[11] Såmark-Roth, A, *et al. Phys. Rev. C*, 98 (2018)
[12] Såmark-Roth, A and Cox, D. M. https://gitlab.com/ASamarkRoth/inpc_2019_suppl (2019)
[13] Ziegler, James F, Ziegler, M. D, and Biersack, J. P. *Nucl. Instrum. Methods Phys. Res. B*, 268:1818–1823 (6 2010)
[14] Pausch, G, Bohne, W, and Hilscher, D. *Nucl. Instrum. Methods Phys. Res. A* (1994)
[15] NNDC. Evaluated Nuclear Structure Data File (ENSDF) Search and Retrieval. http://www.nndc.bnl.gov/ensdf/ (2016)
[16] Eberth, J, *et al. Nucl. Instrum. Methods Phys. Res. A* (1996)
[17] Rudolph, D, *et al. Acta Phys. Pol. B*, 45 (2014)
[18] Lorenz, C. *Ph.D. Thesis*. Lund University (2018). ISBN 978-91-7753-943-8